Acta Crystallographica Section F
Structural Biology and Crystallization Communications
ISSN 1744-3091

Crystallization and X-ray analysis of human cytoplasmic phenylalanyl-tRNA synthetase

Igal Finarov,[a] Nina Moor,[b] Naama Kessler[a] and Mark Safro[a]*

[a]Department of Structural Biology, Weizmann Institute of Science, 76100 Rehovot, Israel, and [b]Institute of Chemical Biology and Fundamental Medicine, 630090 Novosibirsk, Russia

Correspondence e-mail: mark.safro@weizmann.ac.il

Received 15 October 2008
Accepted 12 December 2008

Human cytosolic phenylalanyl-tRNA synthetase (*hc*PheRS) is responsible for the covalent attachment of phenylalanine to its cognate $tRNA^{Phe}$. Significant differences between the amino-acid sequences of eukaryotic and prokaryotic PheRSs indicate that the domain composition of *hc*PheRS differs from that of the *Thermus thermophilus* analogue. As a consequence of the absence of the anticodon-recognizing B8 domain, the binding mode of $tRNA^{Phe}$ to *hc*PheRS is expected to differ from that in prokaryotes. Recombinant *hc*PheRS protein was purified to homogeneity and crystallized. The crystals used for structure determination diffracted to 3.3 Å resolution and belonged to space group *C*2, with unit-cell parameters a = 362.9, b = 213.6, c = 212.7 Å, β = 125.2°. The structure of *hc*PheRS was determined by the molecular-replacement method in combination with phase information from multiwavelength anomalous dispersion.

1. Introduction

Over 100 molecules are directly involved in translation of the genetic code; thus, the progress and efficiency of translation depend on the fine coordination of a large variety of interactions. Among the components of the translational machinery are aminoacyl-tRNA synthetases (aaRSs), which are enzymes that play a key role in protein biosynthesis, catalyzing the aminoacylation of tRNAs with their corresponding amino acids. The attachment of the correct amino acid to tRNA by its synthetase is critical to the fidelity of the translation process.

Human cytoplasmic phenylalanyl-tRNA synthetase (*hc*PheRS) is one of the most complex and the largest enzymes in the aaRS family (for a review, see Safro *et al.*, 2005). *hc*PheRS is a heterotetramer with $(\alpha\beta)_2$ subunit architecture: each dimer is composed of α-subunits and β-subunits consisting of 508 and 589 amino acids, respectively (Moor *et al.*, 2002). Phylogenetic and structural analysis suggests that there are three major forms of PheRS: (i) heterodimeric $(\alpha\beta)_2$ bacterial, (ii) heterodimeric $(\alpha\beta)_2$ archaeal/eukaryotic cytosolic and (iii) monomeric mitochondrial. The heterotetrameric subunit organization of both prokaryotic and eukaryotic cytoplasmic PheRSs is conserved in all species for which sequences are available. However, heterotetrameric organization is not a prerequisite for phenylalanylation activity, as human monomeric mitochondrial PheRS is also active and its structure has been determined recently at 2.2 Å resolution (Klipcan *et al.*, 2008). Thus, eukaryotic cells harbour two different types of PheRSs: cytoplasmic and mitochondrial. The subunit organization of the two enzymes shows marked differences and the binding and recognition modes of the cognate $tRNA^{Phe}$s presumably also differ sharply.

Multiple sequence alignments provide evidence that the polypeptide chains of eukaryotic aaRSs are significantly longer then those of homologous prokaryotic enzymes (Mirande, 1991). Moreover, numerous observations have indicated that elongation of the chains occurs mostly at the N- or C-terminal extremities of the subunits rather than by insertions into the catalytic domain. The sequence of

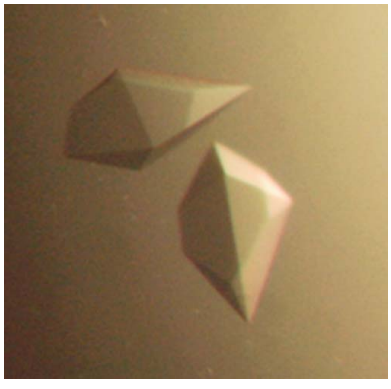

© 2009 International Union of Crystallography
All rights reserved

the *hc*PheRS catalytic α-subunit obeys this rule of thumb: it is ~160 residues longer than the respective prokaryotic analogue, whereas the β-subunit turns out to be ~200 residues shorter (Moor *et al.*, 2002). Multiple sequence alignments clearly outline regions in the α-subunit that are involved in the formation of the active site, thereby confirming that the human α-subunit is indeed catalytic, with general features characteristic of class II aaRSs (Ibba & Soll, 2000).

Although structurally *hc*PheRS belongs to the class II aaRSs, functionally it resembles class I aaRSs, aminoacylating the 2′-OH group of the tRNA terminal ribose. The structure of *Thermus thermophilus* PheRS (Mosyak *et al.*, 1995) complexed with cognate $tRNA^{Phe}$ demonstrates that one $tRNA^{Phe}$ molecule interacts with all four subunits of the enzyme, thus accounting for the enzyme's activity as a functional $(\alpha\beta)_2$ heterotetramer. In bacterial PheRS, recognition and binding of the anticodon triplet of tRNA is mediated by the B8 anticodon-binding domain (RNP) from the β-subunit (Goldgur *et al.*, 1997). In *hc*PheRS, however, no analogues of the RNP domain have been identified in the amino-acid sequence of the β-subunit (Rodova *et al.*, 1999). This finding led to the suggestion that the binding and recognition modes of cognate $tRNA^{Phe}$ differ between prokaryotes and eukaryotes. Together with its canonical aminoacylation and editing functions, *hc*PheRS also possesses some additional functions. For instance, it is responsible for the synthesis and turnover of diadenosine tetraphosphate (Ap_4A), which plays an important role in the response of both bacterial and eukaryotic cells to a variety of stress conditions (Lee *et al.*, 1983). A human mRNA preferentially expressed in human tumorigenic acute-phase chronic myelogenous leukaemia (CML) K562 cells encodes a polypeptide chain identical to the catalytic α-subunit of *hc*PheRS (Rodova *et al.*, 1999; Sen *et al.*, 1997). This is an example of tumour-selective and cell-cycle stage- and differentiation-dependent expression of an aaRS-family member in mammalian cells. The insights provided by structural studies will shed light on the novel amino-acid specificity mode of $tRNA^{Phe}$ binding to human *hc*PheRS and the activities of the enzyme. Here, we report the crystallization, X-ray analysis and molecular-replacement studies of *hc*PheRS and we highlight interesting characteristics of the molecular packing within the crystal asymmetric unit.

2. Materials and methods

2.1. Expression and purification

The two subunits of *hc*PheRS were cloned into two different plasmids: the α-subunit (residues 1–508) was cloned into a pET-21b(+) vector and the β-subunit (residues 1–589) was cloned into a pET-28b(+) vector (Novagen, Germany; Rodova *et al.*, 1999). The presence of a His tag appended to the N-terminus of the β-subunit completely abolished the aminoacylation activity of *hc*PheRS; therefore, no purification tag was used. These two plasmids were co-transformed into *Escherichia coli* strain BLR(DE3) (Novagen, Germany). The purification protocol for the nontagged *hc*PheRS heterotetramer (247 kDa) containing two α-subunits and two β-subunits consisted of five steps. Ammonium sulfate fractionation was followed by four chromatography columns: anion exchange on a DEAE-Sepharose (Amersham Pharmacia Biotech, USA) column (180 ml volume), a heparin-Sepharose CL-6B column (Pharmacia Biotech USA; volume 15 ml), concentrating the protein on a 1 ml TSK hydrophobic interaction column (Tosoh, Japan) and finally gel filtration on a column (0.9 × 45 cm) of superfine Sephadex G-200 (Amersham Pharmacia Biotech, USA; for details, see Moor *et al.*, 2002).

Substitution of the methionines in *hc*PheRS (15 in the α-subunit and 12 in the β-subunit) by selenomethionines (Se-*hc*PheRS) was carried out as described by Van Duyne *et al.* (1993). The protocol used for the purification of Se-*hc*PheRS was similar to that employed for the native protein (Moor *et al.*, 2002).

2.2. Crystallization

Initial crystallization conditions were identified using solutions from Crystal Screens I and II, Index Screen, Cryo Screen, SaltRx (Hampton Research, USA) and PACT Suite (Qiagen, Germany). The microbatch method, performed on an ORYX robot (Douglas Instruments Ltd, London, England; Chayen *et al.*, 1990, 1992), and the hanging-drop vapour-diffusion method were applied. All crystallization experiments were performed at 293 K. *hc*PheRS was concentrated to 2.29 mg ml^{-1} in 20 m*M* Tris–HCl pH 8, 100 m*M* NaCl, 7 m*M* $MgCl_2$, 5 m*M* DTT, 1 m*M* EDTA and 1 m*M* NaN_3. In the hanging-drop vapour-diffusion method, 1 µl protein solution was mixed with 1 µl precipitant solution and equilibrated over a 1 ml reservoir. For microbatch crystallization, 0.3 µl protein solution was mixed with an equal amount of precipitant solution in microbatch 96-well plates and covered with Al's Oil (Hampton Research, USA).

2.3. Data collection

2.3.1. Crystal form I. For data collection, the crystals were transferred to cryoprotectant solution consisting of mother liquor (1.1 *M* sodium citrate pH 6.5, 0.1 *M* MES pH 6.5, 5 m*M* 2-mercaptoethanol and 5 m*M* DTT) supplemented with 20%(*v*/*v*) glycerol and flash-cooled directly in a nitrogen stream at 100 K using a low-temperature

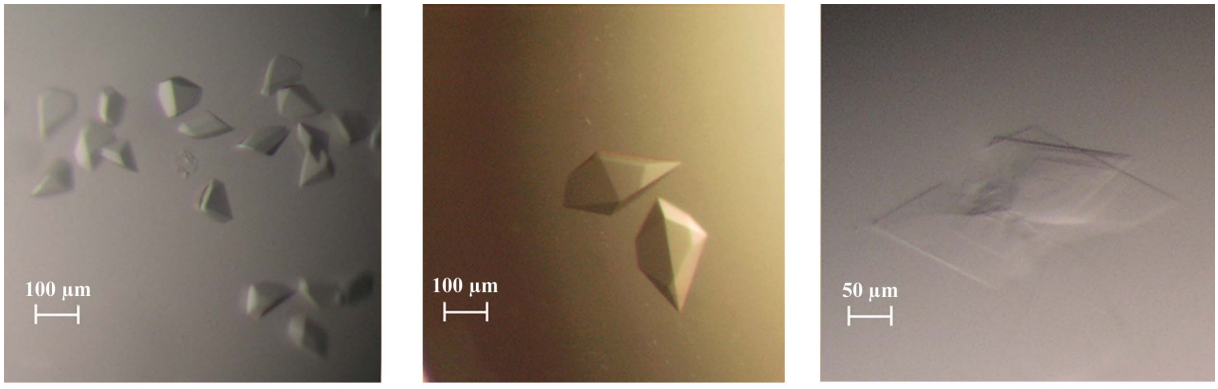

(*a*) (*b*) (*c*)

Figure 1
Three crystal forms of *hc*PheRS: (*a*) crystal form I, (*b*) crystal form II and (*c*) crystal form III.

Table 1
Data-collection statistics for three crystal forms of *hc*PheRS.

Values in parentheses are for the outermost resolution shell.

	Crystal form I				Crystal form II	Crystal form III
Crystal form	Native	SeMet	SeMet	SeMet	Native	Native
Wavelength (Å)	0.934	0.9785 (λ_1†)	0.9788 (λ_2†)	0.8856 (λ_3†)	0.934	0.934
Space group	*C*2				*P*422	*P*2
Unit-cell parameters (Å, °)	a = 362.9, b = 213.6, c = 212.7, $\alpha = \gamma$ = 90.0, β = 125.2				a = 110.9, b = 110.9, c = 290.25, $\alpha = \beta = \gamma$ = 90.0	a = 112.4, b = 383.7, c = 179.9, $\alpha = \gamma$ = 90.0, β = 90.3
Unique reflections	193345 (19201)	110754 (7221)	89030 (5634)	77791 (7775)	15511 (1488)	101570 (6650)
Resolution limits (Å)	30–3.3 (3.42–3.3)	30–4.0 (4.09–4.0)	30–4.3 (4.4–4.3)	30–4.5 (4.66–4.5)	30–4.3 (4.45–4.3)	30–4.1 (4.2–4.1)
Completeness (%)	96.8 (96.8)	99.8 (97.6)	92.8 (60.6)	75.1(22)	98.3 (97.7)	84 (74)
$\langle I/\sigma(I)\rangle$	8.1 (1.23)	10.38 (1.81)	4.7 (1.16)	5.17 (1.8)	10.1 (2.17)	5.49 (2.43)
$R_{\rm merge}$‡	0.071 (0.66)	0.194 (0.692)	0.166 (0.527)	0.165 (0.469)	0.114 (0.663)	0.3 (0.73)
⟨Redundancy⟩	1.9 (1.9)	7.8 (5.6)§	2.0 (1.8)§	2.1 (2.1)§	4.3 (4.3)	3.4 (3.4)

† λ_1, peak; λ_2, inflection point; λ_3, remote wavelength. ‡ $R_{\rm merge}$ is defined as $\sum_{hkl}\sum_i |I_i(hkl) - \langle I(hkl)\rangle|/\sum_{hkl}\sum_i I_i(hkl)$, where $I_i(hkl)$ is the ith observation of reflection hkl and $\langle I(hkl)\rangle$ is the weighted mean of all observations (after rejection of outliers). § Friedel mates separate.

device (Oxford Cryosystems; Cosier & Glazer, 1986). X-ray data were collected to 3.3 Å resolution on the ID14-1 beamline (ESRF, Grenoble, France). Experiments were carried out at a wavelength of 0.933 Å using an oscillation range of 0.25° and a crystal-to-detector distance of 250 mm. The multiwavelength anomalous dispersion (MAD) data set was also collected at the ESRF (BM14 beamline). The X-ray fluorescence spectra at the Se *K* absorption edge were measured prior to MAD data collection. Experimental values of the anomalous scattering factors f' and f'' were derived using the *CHOOCH* program (Evans & Pettifer, 2001). The data were collected at a high-energy remote wavelength as well as at peak and inflection-point wavelengths chosen according to the fluorescence spectrum.

2.3.2. Crystal form II. X-ray data were collected to 4.2 Å resolution at the ESRF (ID29 beamline) at a wavelength of 0.934 Å using an oscillation range of 0.5° and a crystal-to-detector distance of 320 mm.

2.3.3. Crystal form III. X-ray data were collected to 4.1 Å resolution at the ESRF (ID23-I beamline) at a wavelength of 0.934 Å using an oscillation range of 0.5° and a crystal-to-detector distance of 350 mm.

2.4. Data processing

All data sets were processed using the *HKL*-2000 program suite (Otwinowski & Minor, 1996). Matthews parameters (Matthews, 1968; Kantardjieff & Rupp, 2003) were calculated using the *CCP*4 package. The self-rotation function (SRF) was calculated using the *POLARRFN* program (Collaborative Computational Project, Number 4). Molecular-replacement searches were performed using the *AMoRe* (Navaza, 2001), *MOLREP* (Vagin & Teplyakov, 1997), *CNS* (Brünger *et al.*, 1998), *EPMR* (Kissinger *et al.*, 1999) and *Phaser* (McCoy, 2007) programs.

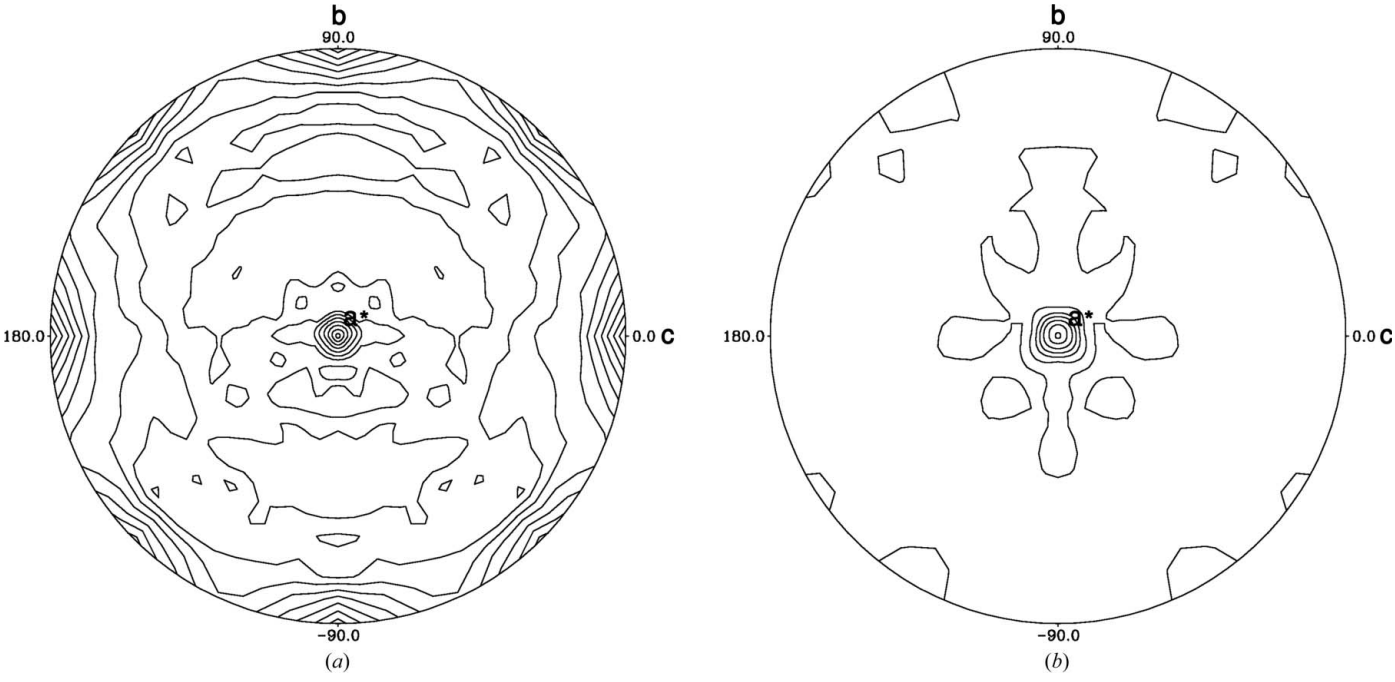

Figure 2
Self-rotation function plots for *hc*PheRS crystal form I (space group *C*2) at sections κ = 180° (*a*) and κ = 90° (*b*). The SRF map was calculated in the resolution range 40–5 Å with an integration radius of 40 Å; the maximal value was normalized to 100 and the contours were drawn at 10-unit intervals beginning at 10.

3. Results and discussion

Three different crystal forms of *hc*PheRS were detected in the crystallization screens (Fig. 1) and characterized using a synchrotron-radiation source at the European Synchrotron Radiation Facility (ESRF, Grenoble, France; see Table 1 for data-collection statistics).

3.1. Crystal form I

Well formed crystals were obtained by the hanging-drop method from a solution containing 1.1 *M* sodium citrate pH 6.5, 0.1 *M* MES pH 6.5, 5 m*M* 2-mercaptoethanol and 5 m*M* DTT. A streak-seeding technique, followed by a number of macroseedings, was used to increase the size of the crystals. These crystals grew to final dimensions of 0.25 × 0.2 × 0.15 mm within three weeks and showed the best diffraction limit (to beyond 3.3 Å resolution) of the three crystal forms (see Fig. 1*a*). The same crystallization conditions were used to grow the crystals of SeMet derivative of *hc*PheRS.

3.2. Crystal form II

Crystals were grown from 20%(*w*/*v*) PEG 3350, 0.1 *M* bis-Tris propane pH 6.5, 5 m*M* 2-mercaptoethanol and 5 m*M* DTT. With macroseeding, these crystals reached final dimensions of 0.4 × 0.3 × 0.2 mm within two weeks (Fig. 1*b*); their diffraction characteristics can be found in Table 1.

3.3. Crystal form III

Crystalline aggregates were obtained from 20%(*w*/*v*) PEG 3350, 0.1 *M* bis-Tris propane pH 6.5, 0.3 *M* sodium malonate, 5 m*M* 2-mercaptoethanol and 5 m*M* DTT. These crystalline aggregates were disintegrated for use in macroseeding experiments. After macroseeding, plate-shaped crystals grew in one week to dimensions of 0.4 × 0.3 × 0.01 mm (Fig. 1*c*).

3.4. Molecular replacement studies

The crystallization conditions for crystal forms II and III were first obtained by the microbatch technique and then applied to hanging drops in order to grow the crystals to their final dimensions. Macroseeding for all three crystal forms was performed by lowering the concentration of precipitant by 5%.

Form I crystals of *hc*PheRS grew in space group *C*2, with unit-cell parameters $a = 362.9$, $b = 213.6$, $c = 212.7$ Å, $\alpha = \beta = 90.0$, $\gamma = 125.2^\circ$. These crystals were selected for subsequent structure determination (see Table 1). V_M values for form I crystals ranged between 2.3 and 4.5 Å^3 Da^{-1}, corresponding to a solvent content of between 45.5 and 72.7%. This suggests that there are *M* copies of the *hc*PheRS molecule in an asymmetric unit, where $6 \geq M \geq 3$. However, only peaks corresponding to one fourfold axis and five twofold axes could be clearly seen on the self-rotation function maps. Stereographic projections of the self-rotation map in polar coordinates for $\kappa = 90^\circ$ and $\kappa = 180^\circ$ are presented in Fig. 2.

At first glance, the appearance of a fourfold noncrystallographic axis suggests the presence of four molecules in the asymmetric unit related by noncrystallographic symmetry (NCS) elements. Four *hc*PheRS molecules within an asymmetric unit correspond to a V_M value of 3.4 Å^3 Da^{-1} and a solvent content of 63.3%.

Within the context of the MAD experiments, three data sets (at the peak, the inflection point and a remote wavelength) were collected for crystal form I of selenomethionine-labelled *hc*PheRS. However, despite the use of various programs (listed in §2.4), we failed to automatically locate the positions of 216 Se atoms in the four molecules within the asymmetric unit. It seems likely that the number of Se atoms, coupled with the strength of the anomalous signal, preclude their automatic identification.

Therefore, molecular replacement was implemented for phase determination. The atomic coordinates of *T. thermophilus* PheRS (PDB code 1pys; Mosyak *et al.*, 1995) and a β-subunit fragment of *Pyrococcus horikoshii* PheRS (PDB code 2cxi; Sasaki *et al.*, 2006) were used to construct a preliminary model and to carry out an initial search. The model comprised 71.1% of the total number of *hc*PheRS amino-acid residues; 29% of them share identity with the *hc*PheRS sequence. All side chains were substituted to serines. We first searched for the positions of $(\alpha\beta)_2$ tetramers in the asymmetric unit of the form I crystals. Notably, from the multiple sequence alignment we derived the presence of motif 1 in the amino-acid sequence of *hc*PheRS. This motif is characterized by a relatively long α-helix followed by a β-strand and is implicated in the interface formation of dimers and tetramers in class II aaRS. Thus, we believe that the intersubunit interface of *hc*PheRS will also display the topology of the four-helix bundle observed in the *T. thermophilus* structure (Mosyak *et al.*, 1995). Within the asymmetric unit (ASU), the number of tetramers searched varied from one to four (as was to be expected from the self-rotation function). However, we failed to find a solution without steric hindrance. In the next stage of the molecular-replacement search, we used an $(\alpha\beta)$ heterodimer as the basis of our model. In a similar manner, we varied the number of $(\alpha\beta)$ heterodimers searched for in the ASU. One of the solutions suggested by the *Phaser* program (McCoy, 2007) perfectly resembled the $(\alpha\beta)_2$ subunit organization of *T. thermophilus* PheRS. However, despite the apparent similarity between the *T. thermophilus* tetramer and that found by molecular replacement, differences in the relative orientations of the two heterodimers forming prokaryotic and eukaryotic $(\alpha\beta)_2$ molecules were detected.

The changes in the relative orientations of the two heterodimers induced steric clashes between the structural fragments (β592–β603) related by an intramolecular twofold axis. In the subsequent stages of model rebuilding and refinement, this fragment was removed from the coordinate file. A molecular-replacement search for four modified tetramers in the ASU using the *Phaser* program provided us with a final high *Z* score (23.4) solution.

The model obtained from this molecular-replacement search clearly showed that the fourfold axis observed in the rotation-function map is a pseudo-NCS element. In fact, *hc*PheRS molecules

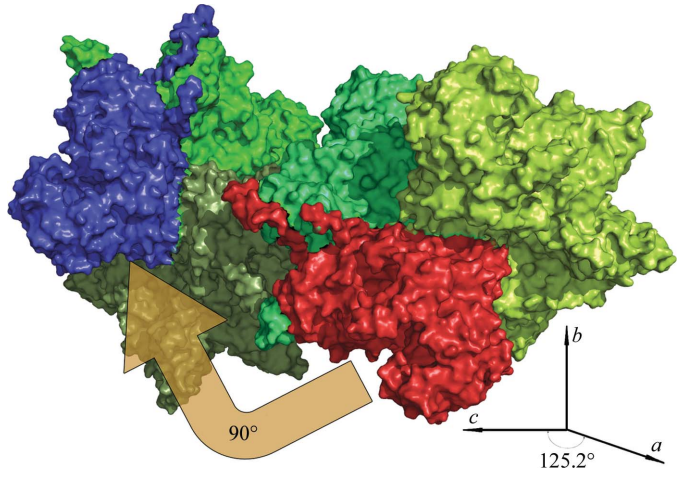

Figure 3
Pairs of heterodimers located in different tetramers (shown in red and blue) are related by a rotation of 90°, inducing the appearance of a peak at $\kappa = 90^\circ$ on the SRF map.

crystallize as dimers of two $(\alpha\beta)_2$ heterotetramers. Two such dimers are in turn also related by a twofold NCS axis. There is also a twofold intramolecular axis relating the two heterodimers inside the heterotetramers. The combination of all NCS elements in the asymmetric unit generates a fourfold NCS axis, as seen in the SRF map at $\kappa = 90^\circ$ (Fig. 3).

The structure of *hc*PheRS, in complex with its endogenous ligand phenylalanine, has now been determined by a combination of molecular-replacement and multiwavelength anomalous dispersion methods. The refinement of the human cytoplasmic PheRS structure is currently in progress and will be reported elsewhere.

This work was supported by Binational Science Foundation Grant No. 2005209 (to MS), by the Kimmelman Center for Biomolecular Structure and Assembly at WIS (to MS) and by grant 06-04-48798 from the Russian Foundation for Basic Research (to NM).

References

Brünger, A. T., Adams, P. D., Clore, G. M., DeLano, W. L., Gros, P., Grosse-Kunstleve, R. W., Jiang, J.-S., Kuszewski, J., Nilges, M., Pannu, N. S., Read, R. J., Rice, L. M., Simonson, T. & Warren, G. L. (1998). *Acta Cryst.* D**54**, 905–921.
Chayen, N. E., Shaw Stewart, P. D. & Blow, D. M. (1992). *J. Cryst. Growth*, **122**, 176–180.
Chayen, N. E., Shaw Stewart, P. D., Maeder, D. L. & Blow, D. M. (1990). *J. Appl. Cryst.* **23**, 297–302.
Cosier, J. & Glazer, A. M. (1986). *J. Appl. Cryst.* **19**, 105–107.
Evans, G. & Pettifer, R. F. (2001). *J. Appl. Cryst.* **34**, 82–86.
Goldgur, Y., Mosyak, L., Reshetnikova, L., Ankilova, V., Lavrik, O., Khodyreva, S. & Safro, M. (1997). *Structure*, **5**, 59–68.
Ibba, M. & Soll, D. (2000). *Annu. Rev. Biochem.* **69**, 617–650.
Kantardjieff, K. A. & Rupp, B. (2003). *Protein Sci.* **12**, 1865–1871.
Kissinger, C. R., Gehlhaar, D. K. & Fogel, D. B. (1999). *Acta Cryst.* D**55**, 484–491.
Klipcan, L., Levin, I., Kessler, N., Moor, N., Finarov, I. & Safro, M. (2008). *Structure*, **16**, 1095–1104.
Lee, P. C., Bochner, B. R. & Ames, B. N. (1983). *Proc. Natl Acad. Sci. USA*, **80**, 7496–7500.
Matthews, B. W. (1968). *J. Mol. Biol.* **33**, 491–497.
McCoy, A. J. (2007). *Acta Cryst.* D**63**, 32–41.
Mirande, M. (1991). *Prog. Nucleic Acid Res. Mol. Biol.* **40**, 95–142.
Moor, N., Linshiz, G. & Safro, M. (2002). *Protein Expr. Purif.* **24**, 260–267.
Mosyak, L., Reshetnikova, L., Goldgur, Y., Delarue, M. & Safro, M. G. (1995). *Nature Struct. Biol.* **2**, 537–547.
Navaza, J. (2001). *Acta Cryst.* D**57**, 1367–1372.
Otwinowski, Z. & Minor, W. (1996). *Methods Enzymol.* **276**, 307–326.
Rodova, M., Ankilova, V. & Safro, M. G. (1999). *Biochem. Biophys. Res. Commun.* **255**, 765–773.
Safro, M. G., Moor, N. & Lavrik, O. (2005). *The Aminoacyl-tRNA Synthetases*, edited by M. Ibba, C. Francklyn & S. Cusack, pp. 250–265. Austin, USA: Landes Bioscience.
Sasaki, H. M., Sekine, S., Sengoku, T., Fukunaga, R., Hattori, M., Utsunomiya, Y., Kuroishi, C., Kuramitsu, S., Shirouzu, M. & Yokoyama, S. (2006). *Proc. Natl Acad. Sci. USA*, **103**, 14744–14749.
Sen, S., Zhou, H., Ripmaster, T., Hittelman, W., Schimmel, P. & White, R. (1997). *Proc. Natl Acad. Sci. USA*, **94**, 6164–6169.
Vagin, A. & Teplyakov, A. (1997). *J. Appl. Cryst.* **30**, 1022–1025.
Van Duyne, G. D., Standaert, R. F., Karplus, P. A., Schreiber, S. L. & Clardy, J. (1993). *J. Mol. Biol.* **229**, 105–124.